ECS Transactions, 57 (1) 1371-1378 (2013)
10.1149/05701.1371ecst ©The Electrochemical Society

Spin-coated $La_{0.8}Sr_{0.2}Ga_{0.8}Mg_{0.2}O_{3-\delta}$ Electrolyte on Infiltrated Anodes for Direct Methane Fuel Cells

Z. Salehi[a], I. Luisetto[b], F. Basoli[a], A. D'Epifanio[a], S. Licoccia[a], S. Tuti[b] and E. Di Bartolomeo[a]

[a]Department of Chemical Science and Technology and NAST Center, University of Rome Tor Vergata, Via della Ricerca Scientifica 1, 00133 Rome, Italy
[b]Department of Science, University of Rome "Roma Tre", Via dellaVasca Navale 79, 00146 Rome, Italy

Dense micrometric $La_{0.8}Sr_{0.2}Ga_{0.8}Mg_{0.2}O_{3-\delta}$ (LSGM) films were deposited by spin-coating on porous LSGM scaffolds characterized by homogeneous pore structure. Porous anodes were infiltrated with aqueous nickel and nickel/copper nitrate solutions, dried and fired at 700°C. Homogeneous metal coating with proper interconnection was observed by SEM, chemical stability was confirmed by XRD, and electrical characterization of anodic substrates was performed. Catalytic activity of different anodes was evaluated ex-situ in a quartz micro-reactor fed with CH_4:CO_2 mixtureat range 650 and 700°C. To investigate the redox properties of the metallic phases, the anodic substrates were subjected to redox ageing cycles and characterized by H_2-TPR.

Introduction

$La_{0.8}Sr_{0.2}Ga_{0.8}Mg_{0.2}O_{3-\delta}$ (LSGM) has emerged as one of the most promising electrolyte for Intermediate Temperature Solid Oxide Fuel Cells (IT-SOFC) application because of its high ionic conductivity at reduced temperatures, negligible electronic conduction and a good stability over a wide range of oxygen partial pressure (1-10). Its major drawback is a fair chemical stability with the other fuel cell components: the reactivity with Ni present at the anode side to form insulating phases and cation interdiffusion with typical perovskite oxide commonly used such as $La_{1-x}Sr_xMnO_{3-\delta}$ (LSM) and $La_{1-x}Sr_xFe_yCo_{1-y}O_{3-\delta}$ (LSFC) at the cathode side.

The performance at 800 °C are excellent reaching 1.4 W/cm^2 of power output for a 200 micron thick electrolyte based cell (11,12), while decreasing the operating temperature, the performance abruptly decreased because of the large ohmic resistance losses and the increasing polarization resistance. Thus, decreasing the electrolyte thickness is highly required to deliver high power output at IT. Recently, many attempts have been made to reduce the LSGM electrolyte thickness (13,17); in this work, micrometric dense LSGM films were deposited by spin-coating method on porous LSGM anodic substrates. The spin coating technique is cost effective and efficient method for anode supported single cell fabrication (18).

LSGM scaffold with homogeneous and porous microstructure were used as anodic substrates for film deposition. After the co-sintering process, the LSGM scaffolds were infiltrated with nickel and nickel-coppernitrate solutions (50:50) and then calcined.

The reduction behavior of composite anodes was studied by H_2-TPR. In order to evaluate the occurrence of methane cracking or CO_2 reforming, the anodic substrates were exposed to CH_4:CO_2 mixtures at 650 and 700 °C.

Experimental

LSGM commercial powders by Praxair (5 m^2g^{-1}) were used for fabrication of both anode and spun electrolyte layers.

Supporting anodes were prepared by die pressing method: LSGM and BUTVAR 98 (Sigma Aldrich) (5 wt%) used as binder were planetary ball milled in ethanol solvent at 350 rpm for 1 h. Micrometric graphite (Sigma Aldrich) was added as pore forming agent and planetary milled at 250 rpm for 30 min. The slurry was dried at 80 °C overnight; the resulting powder was grounded in an agate mortar and uniaxially pressed at 100 MPa into cylindrical pellets of 12 mm in diameter. The porous pellets were pre-sintered at 1200°C for 6 h with heating rate of 5°C/min.

Dense LSGM membranes were fabricated by spin coating technique. LSGM (25 wt%) was planetary milled in organics solvent (terpineol:ethanol 1:1 vol%) with BUTVAR 98 as binder (5 wt%) and polyethylene glycol PEG400 (3 wt%) and di-n butyl phthalate DBP (3 wt%) as plasticizers to form a stable colloidal slurry. A stable LSGM containing colloidal slurry was obtained by milling the components for 20 h at 350 rounds min^{-1} (higher rates were avoided to prevent overheating of the slurry). The pre-sintered anodes were vacuum fixed on the chuck of the coater (Laurell model WS-400-6NPP) and the electrolyte slurry was spin coated at a rotating speed of 6 krpm for 30 s. The coated substrate was dried at 80°C for 30 min and thermally treated after 3 depositions at 400°C for 1 h to remove the organics. The spin coating process was repeated until the desired electrolyte thickness was obtained. The half cell was co-sintered at 1450 °C for 6 h.

To introduce the catalytic component into the anodic substrates, the LSGM porous scaffolds were impregnated by a 4 M aqueous solution of Nickel nitrate (purity 99% by Aldrich) or Nickel-Copper nitrates (50:50 wt%) then calcined at 700 °C for 30 min.

The amount of the deposited NiO or NiO-CuO catalysts was evaluated by the percentage weight increase after each impregnation/calcination cycle. Finally, NiO was reduced to Ni upon hydrogen exposure.

Structural and morphological characterizations of powders, pellets and half cells were performed by X-ray diffraction (XRD) analysis (Philips X-Pert Pro 500 Diffractometer) and field emission scanning electron microscopy (FE-SEM, Leo Supra 35).

The catalytic activity (Ex Situ) of each impregnated anode was measured in a test ring equipped with mass flow controller and a quartz tubular reactor at atmospheric pressure. CH_4/CO_2 ratio of 1 was fed into reactor using 75000 ml g^{-1} h^{-1} (GHSV) at 650 and 700 °C. Prior to catalytic activity, samples were reduced flowing 50%H_2/Ar for 1 h at 700 °C. Gas composition was analyzed by gas chromatograph (Varian, star 3400 CX) equipped with a TCD detector.

Temperature programmed reduction (TPR) experiments were performed by a Thermo Scientific TPDRO1100 flow apparatus. The H_2 consumption was measured by a TCD detector. Impregnated anodes were pre-treated in a flow of 10% O_2/He mixture (20 cm^3 min^{-1}) at 700 °C for 30 min, and then cooled in He to RT. Then, a 5% H_2/Ar mixture (10 cm^3 min^{-1}) was flowed through the sample starting at 500°C and heating up to a final temperature of 700 °C, with a rate of 10 °C min^{-1}. The catalytic activity was measured in a fixed-bed quartz reactor at atmospheric pressure connected to a flow apparatus equipped with mass flow controllers.

Results and Discussion

To get proper porosity, different amounts of micrometric carbon between 40 and 55 wt% were mixed with LSGM powder. Fig. 1 a) and b) shows the SEM images of the cross section of sintered (1450°C for 6 h) anodic substrates containing 40 and 55 wt% of micrometric carbon at the same magnification. The sample containing 40 wt% of carbon shows micrometric pores without interconnections while the sample with 55 wt% of carbon has larger and interconnected pores homogenously dispersed suitable for consequent infiltration of catalysts. LSGM scaffold is well sintered as shown by the necking between the grains and interconnected pores of about 10 μm are clearly visible.

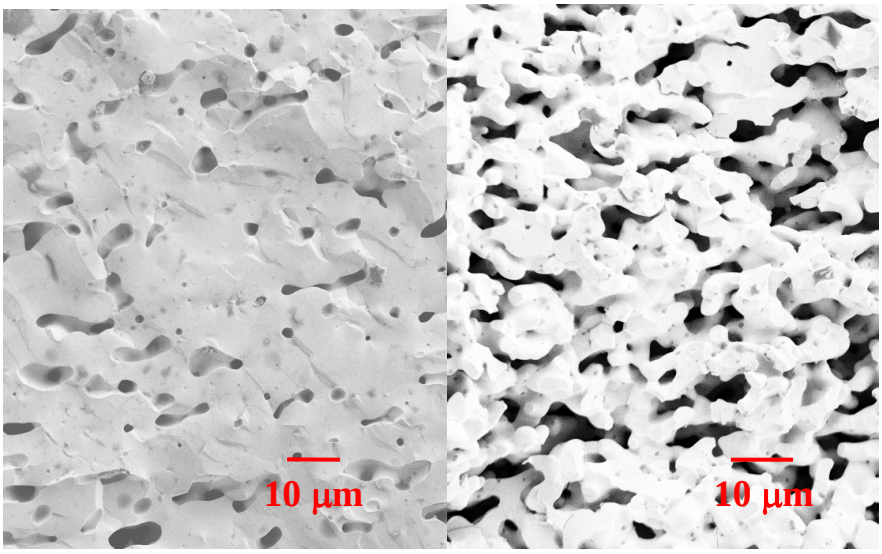

Figure 1. SEM micrographs of cross section of sintered LSGM scaffold containing a) 40 and b) 50 wt% of micrometric carbon.

600 μm porous pre-sintered anodic pellets were prepared as substrates for the spin-coated LSGM layers. After the deposition of each layer, the sample was dried at 80°C for

30 min and thermally treated at 400°C for 1 h to remove the organics and avoid the formations of pinholes after three spun layers.

The co-sintering at 1450°C for 6 h of the pre-sintered anodic substrate and the deposited layers ensure a porous LSGM scaffold with a dense LSGM membrane.

In Fig. 2, the SEM micrograph of top view of LSGM layer is reported. A fully dense LSGM membrane is clearly noticeable and no open porosity was detected. A small dark second phase is detected in the deposited LSGM layer (but also in the pellets sintered at the same temperature) both at the grain-boundary and in the bulk as already reported in the literature (19).

The XRD pattern shown in Fig. 3 of deposited LSGM membrane failed to discern the second phase, confirming the presence of LSGM single phase, implying that the amount of the second phase in below the detection limit of XRD, e.g. 5 wt%.

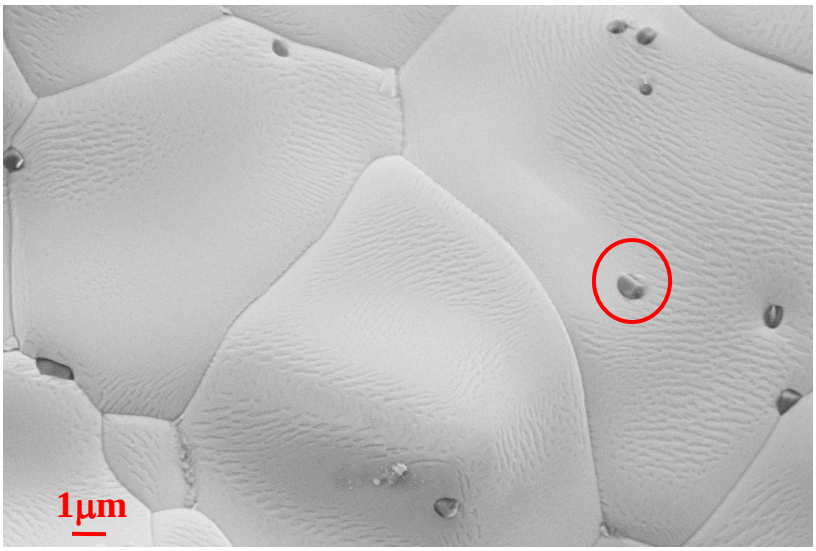

Figure 2. SEM micrograph of top view of sintered LSGM spun membrane.

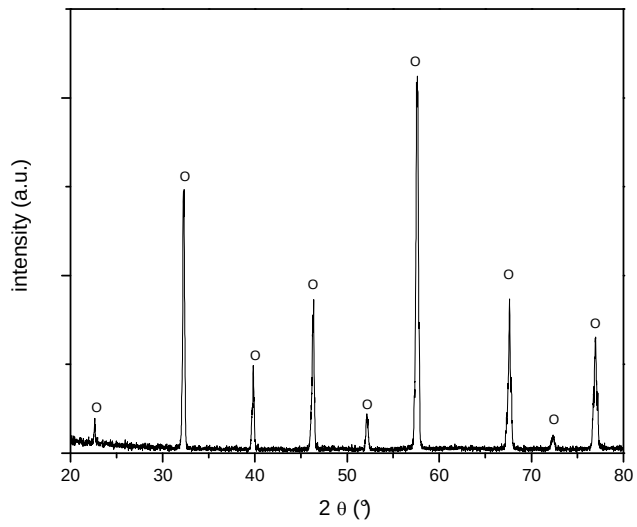

Figure 3. XRD pattern of deposited LSGM layer after co-sintering at 1450°C.

The thickness of the electrolyte membrane can be controlled by: viscosity of slurry, spin-coating velocity and number of spun layers. LSGM films of different thickness from 5-7 to 12-15 μm, were obtained by using 5 or 15 spun layers, respectively.

Figure 4 shows the SEM micrographs of the surface fracture of 5 layers and 15 layers LSGM deposited films on the LSGM substrate. The electrolytes showed thicknesses of about 5-6 μm (Fig. 4(a)) and 15 μm (Fig. 4(b)) revealing that each spun correspond to 1 μm and thus the electrolyte thickness can be carefully controlled. Moreover the micrographs show a good adhesion between the electrolyte and the anodic support, revealing microstructures free of cracks and fully densified. Furthermore, the anodic supports showed an appropriate micrometric porosity.

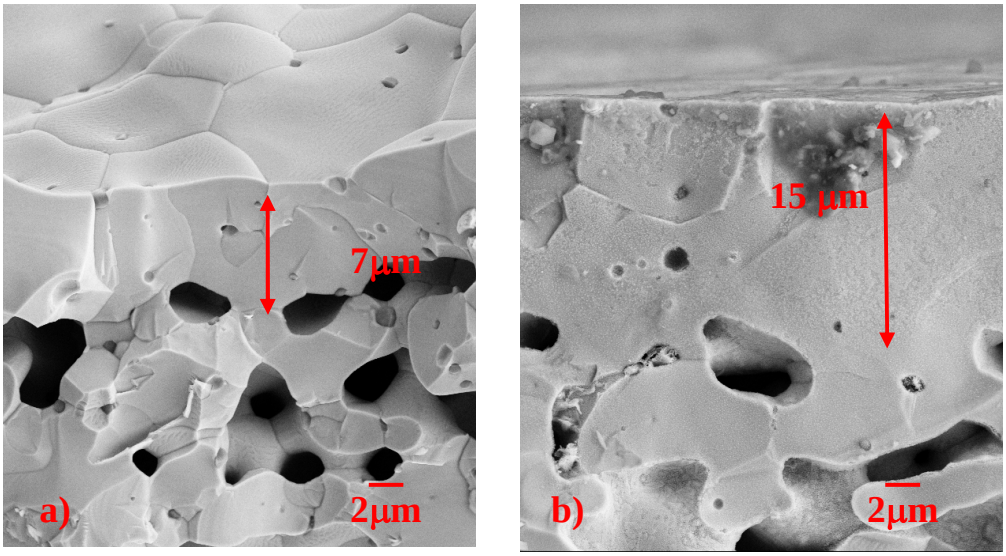

Figure 4. SEM micrographs (cross section) of 5 and 15 spun LSGM membranes

Nickel nitrate was deposited on the internal surfaces of the porous LSGM scaffold by infiltration of ~~an~~ 4M aqueous solution of nickel nitrate. To obtain NiO~~a~~ calcinations, treatment at 700 °C for 30 min in air was performed.

Multiple impregnation/calcination cycles were necessary to introduce a proper amount of catalytic oxide into the LSGM scaffolds. A single impregnation/calcination cycle yielded a NiO weight loading (W_{NiO}) of 0.8% in the porous LSGM scaffold.

To define the reduction treatment, H_2-TPR analysis of infiltrated anodes was performed and reported in Fig 5. NiO-LSGM showed a main reduction peak at 445°C assigned to the reduction of bulk NiO which has a low interaction with the LSGM scaffold, and a weak peak at about 630°C related to the reduction of NiO species strongly interacting with the scaffold. NiO-CuO-LSGM showed a narrow and intense reduction peak at temperature much lower (284°C) than that of NiO-LSGM anode, which is attributed to the simultaneous reduction of NiO and CuO oxides. The H_2-TPR analysis suggests that the presence of CuO markedly enhances the reducibility of NiO. The treatment in hydrogen up to 700°C yielded the full reduction of NiO and CuO species to Ni and Cu metals.

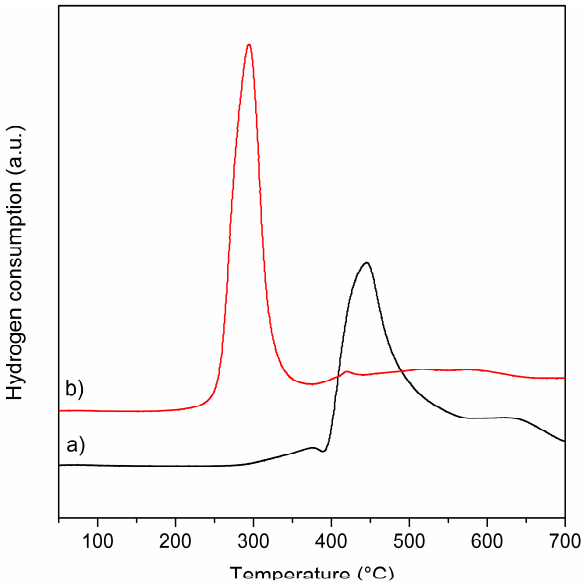

Figure 5. H_2-TPR profile of NiO-LSGM (a) and NiO-CuO-LSGM (b) anodes

Figure 6 shows a SEM micrograph of the cross section of NiO-LSGM anode after 12 impregnations (corresponding at 10 %wt of NiO loading) and after the reduction treatment at 700°C for 2h. Ni layer consisting of nanometric grains is quite porous but well interconnected and uniformly coats the pore walls of LSGM scaffold. The Ni particles interconnection ensures a good percolation path for the electronic conduction.

In Fig. 7, X-Ray diffraction pattern of the infiltrated anode showed the existence of Ni and LSGM phases after hydrogen reduction and no evidence of secondary phases was revealed. The low temperature (700°C) used to form NiO after the infiltration allowed to get a good chemical compatibility between the infiltrate catalyst coating and the LSGM backbone.

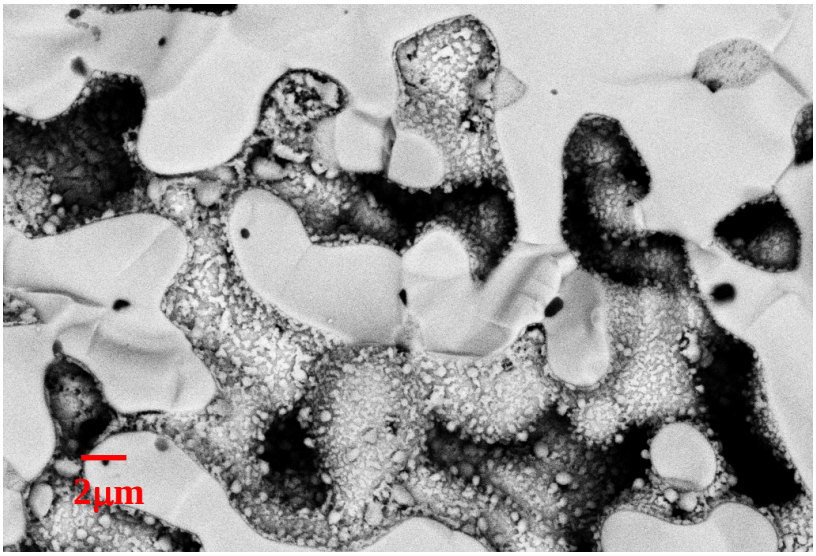

Figure 6. SEM micrograph of cross section of Ni infiltrated LSGM scaffold after reduction in H_2 at 700 °C

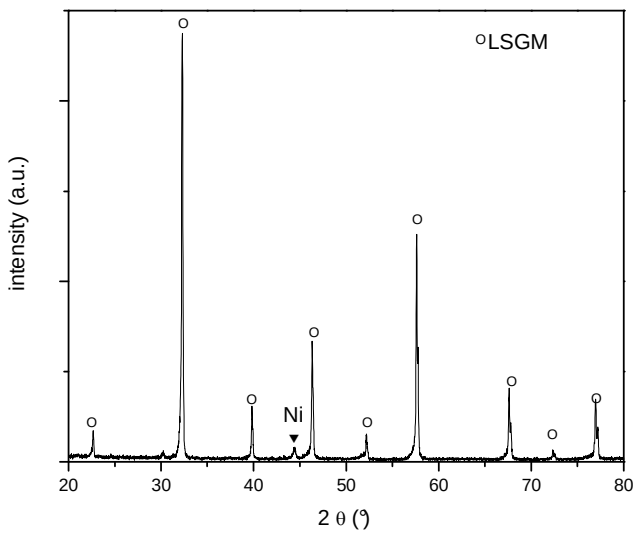

Figure7. XRD pattern of Ni infiltrated LSGM anode

Finally, to evaluate the occurrence of methane cracking or CO_2 reforming, the anodic substrate was exposed to a CH_4:CO_2 mixture. A mixture of CH_4:CO_2=1 with a gas hour space velocity (GHVS) = 75000 mL $h^{-1}g^{-1}$ was flowed over the anodes at 650 and 700°C. The CH_4 conversion to CO and H_2 was 20% on NiO-LSGM and 13 % on CuO-NiO-LSGM at 700°C. The CH_4 conversion decreased to 13% on NiO-LSGM and was almost zero on CuO-NiO-LSGM at 650°C. These results show that Cu is inactive toward the CH_4 cracking and the CO_2 reforming of CH_4, suggesting a higher resistance to carbon formation of NiO-CuO-LSGM composite with respect to NiO-LSGM. However, a proper catalytic activity of CO_2 reforming of CH_4 is beneficial to enhance the electrocatalytic activity of the anodes, thus a further investigation on the proper composition of the anodic additive that should have high selectivity and activity toward CO_2 reforming of CH_4 is required.

Conclusions

Micrometric LSGM electrolyte layers were deposited by slurry spin coating on LSGM anodic scaffold with an appropriate micrometric porosity. Highly-porous LSGM scaffolds were infiltrated via impregnation of aqueous nickel and nickel-copper nitrate solutions and calcined at 700 °C. No secondary phases were revealed.

Due to the fine-grained microstructures and the homogenous distribution of Ni nanoparticles, the anodes prepared through infiltration are easily reducible and a much lower Ni content may provide an adequate electrical conductivity.

From catalytic investigation, a proper composition of the anodic additive with high selectivity and activity toward CO_2 reforming of CH_4 might be developed.

Acknowledgments

The authors acknowledge the Italian Ministry of Research and Education within the program "Programmi di Ricerca Scientifica di Rilevante Interesse Nazionale-PRIN-Anno 2010-2011–Prot. 2010KHLKFC".

References

1. M. Feng and J. B. Goodenough, *Eur. J. Solid State Inorg. Chem*., **31**, 663 (1994).
2. T. Ishihara, H. Matsuda, and Y. Takita, *J. Am. Chem. Soc*., **116**, 3801 (1994).
3. T. Ishihara, H. Matsuda, and Y. Takita, *Solid State Ionics*, **79**, 147 (1995).
4. K. Huang, M. Feng, and J. Goodenough, *J. Am. Ceram. Soc*., **79**, 1100 (1996).
5. P. Huang and A. Petric, *J. Electrochem. Soc.*, **143**, 1644 (1996).
6. J. W. Stevenson, T. R. Armstrong, D. E. McCready, L. R. Pederson, and W. J. Weber, *J. Electrochem. Soc*., **144**, 3613 (1997).
7. K. Huang, M. Feng, J. B. Goodenough, and C. Milliken, *J. Electrochem. Soc*., **144**,3620 (1997).
8. K. Huang, R. Tichy, J. B. Goodenough, and C. Milliken, *J. Am. Ceram. Soc*., **81**,2565 (1998).
9. K. Huang, R. Tichy, J. B. Goodenough, and C. Milliken, *J. Am. Ceram. Soc*., **81**,2581 (1998).
10. J.H. Wan, J.Q. Yan, and J.B. Goodenough, *J. Electrochem. Soc*., **152**, A-1511 (2005).
11. X.C. Lu and J.H. Zhu, *J. Electrochem. Soc*.,**155** (5), B494 (2008).
12. Y.B. Lin and S.A. Barnett, *Electrochem*. *Solid-State Lett*., **9**,A285 (2006).
13. W.M. Guo, J. Liu, and Y.H. Zhang, *Electrochim. Acta*, **53**,4420 (2008).
14. Z.H. Bi, B.L. Yi, Z.W. Wang, Y.L. Dong, H.J. Wu, Y.C. She, and M.J. Cheng, *Electrochem. Solid-State Lett.*,**7**, A105 (2004).
15. J.W. Yan, H. Matsumoto, M. Enoki, and T. Ishihara, *Electrochem. Solid-State Lett.*,**8**A, 389 (2005).
16. T. Ishihara, J.W. Yan, M. Shinagawa, and H. Matsumoto, *Electrochim. Acta,* **52,** 1645 (2006).
17. J.W. Yan, H. Matsumoto, T. Akbay, T. Yamada, and T. Ishihara, *J. Power Source,* **157**,714 (2006).
18. X. Ding, J. Gu, D. Gao, G. Chen, and Y. Zhang, *J. Power Source,***195,** 4252 (2010).
19. X. Zhao, X. Li, N. Xu, and K. Huang, *Solid State Ionics*, **214**, 56 (2012).